Title: Quantitative Analysis Of Lipid Debris Accumulation Caused By Cuprizone Induced Myelin Degradation In Different Cns Areas

Authors: Attila Ozsvár, Róbert Szipőcs, Zoltán Ozsvár, Judith Baka, Pál Barzó, Gábor Tamás, Gábor Molnár

PII: S0361-9230(17)30436-7
DOI: https://doi.org/10.1016/j.brainresbull.2018.01.003
Reference: BRB 9352

To appear in: *Brain Research Bulletin*

Received date: 31-7-2017
Revised date: 22-12-2017
Accepted date: 4-1-2018

Please cite this article as: Attila Ozsvár, Róbert Szipőcs, Zoltán Ozsvár, Judith Baka, Pál Barzó, Gábor Tamás, Gábor Molnár, Quantitative Analysis Of Lipid Debris Accumulation Caused By Cuprizone Induced Myelin Degradation In Different Cns Areas, Brain Research Bulletin https://doi.org/10.1016/j.brainresbull.2018.01.003

QUANTITATIVE ANALYSIS OF LIPID DEBRIS ACCUMULATION CAUSED BY CUPRIZONE INDUCED MYELIN DEGRADATION IN DIFFERENT CNS AREAS

Attila Ozsvár[1], Róbert Szipőcs[2,3], Zoltán Ozsvár[4], Judith Baka[1], Pál Barzó[5], Gábor Tamás[1], Gábor Molnár[1*]

[1]MTA-SZTE Research Group for Cortical Microcircuits, Department of Physiology, Anatomy and Neuroscience, University of Szeged, Közép fasor 52, Szeged, H-6726, Hungary

[2]Department of Applied and Nonlinear Optics, Institute for Solid State Physics and Optics, Konkoly-Thege M. u. 29-33, Budapest, H-1525, Hungary.

[3]R&D Ultrafast Lasers Ltd, Budapest, H-1539 Budapest, Hungary

[4]Department of Image Processing and Computer Graphics, University of Szeged, Árpád tér 2, Szeged, H-6720, Hungary

[5] Department of Neurosurgery, University of Szeged, Semmelweis u. 6., Szeged, H-6725, Hungary

**Correspondence: molnarg@bio.u-szeged.hu*

Highlights

- Lipid debris accumulation was detected after demyelination with cuprizone
- Quantification of lipid debris showed gradual increase over time
- Amount of lipid debris is brain region dependent
- Detection of lipid debris is capable to reveal early phase of demyelination

ABSTRACT

Degradation of myelin sheath is thought to be the cause of neurodegenerative diseases, such as multiple sclerosis (MS), but definitive agreement on mechanism of how myelin is lost is currently lacking. Autoimmune initiation of MS has been recently questioned by proposing that the immune response is a consequence of oligodendrocyte degeneration. To study the process of myelin breakdown, we induced demyelination with cuprizone and applied coherent anti-Stokes Raman

scattering (CARS) microscopy, a non-destructive label-free method to image lipid structures in living tissue. We confirmed earlier results showing a brain region dependent myelin destructive effect of cuprizone. In addition, high resolution *in situ* CARS imaging revealed myelin debris forming lipid droplets alongside myelinated axon fibers. Quantification of lipid debris with a custom-made software for segmentation and three dimensional reconstruction revealed brain region dependent accumulation of lipid drops inversely correlated to the thickness of myelin sheaths. Finally, we confirmed that *in situ* CARS imaging is applicable to living human brain tissue in brain slices derived from a patient. Thus, CARS microscopy is potent tool for quantitative monitoring of myelin degradation at unprecedented spatiotemporal resolution during oligodendrocyte damage. We think that accumulation of lipid drops around degrading myelin might be instrumental in triggering subsequent inflammatory processes.

Abbreviations

BODIPY boron-dipyrromethene

Keywords: Multiple sclerosis; Cuprizone; Demyelination; Lipid debris; CARS imaging

Introduction

Multiple sclerosis (MS) is a disease of oligondendrocyte and myelin sheath affecting both the white and gray matter with diverse symptoms such as tremor, fatigue and paralysis (Hemmer et al., 2002; Trapp and Nave, 2008). In most cases the symptoms occur in a relapsing-remitting manner which usually devolves into a persistent progressive state after a decade following onset. MS is caused by demyelination and inflammation of axonal tracts. Since myelin acts as an insulator, injury of myelin sheaths wrapped around axons of neurons in the CNS it causes malfunction by impairing conduction of electric signals (Bando et al., 2008; Hamada and Kole, 2015). Moreover, the loss of myelin cause

axonal (Huizinga et al., 2012; Kuhlmann et al., 2002; Lindner et al., 2009) and finally neuronal degeneration (Centonze et al., 2010).

The precise pathological mechanisms involved in MS are subject to considerable debate. Commonly MS is defined as an autoimmune disease initiated by an immune system dysregulation leading autoreactive T cells to enter the brain, induce microglia and macrophages to attack and erode myelin which finally causes the injury of oligondendrocytes (Frohman et al., 2006; Kornek and Lassmann, 2003; Stadelmann et al., 2011). This theory is corroborated by the fact that current effective treatments of MS are based on anti-inflammatory and immunomodulatory agents. Immune dysregulation is also supported by the results of genome-wide association (GWAS) studies showing an excessive number of genes influencing T-cell differentiation (Sawcer et al., 2011). However, mechanisms of MS initiation are still hypothetical and multiple factors such as gender, viral infection, genetic predisposition, environmental and living circumstances were suggested as potential contributors (Simpson et al., 2015). An alternative hypothesis for the etiology has been proposed due to lack of lymphocytic infiltrates in early lesions (Barnett and Prineas, 2004). It was suggested that death of the oligodendrocyte may the primary problem of disease and autoreactivity against due to release of myelin debris causing more inflammation and further demyelination (Clarner et al., 2012; Stys et al., 2012; Traka et al., 2015).

Disease models of human demyelination include genetically modified animals, virus and toxin induced demyelination and the most frequent rodent model of MS, experimental autoimmune encephalomyelitis (EAE) (Merrill, 2009; Ransohoff, 2012). The latter is in agreement with the autoimmune disease initiated theory by using an oligodendrocyte specific protein as an antigenic component to generate autoreaction against myelin. The present study induces demyelination initiated by the loss of olygodendrocytes by using cuprizone as an effective apoptotic agent disrupting the energy metabolism of oligodendrocytes through copper depletion (Acs and Kalman, 2012; Gudi et al., 2014; Kipp et al., 2009; Matsushima and Morell, 2001; Skripuletz et al., 2011)

leading to the disintegration of myelin sheath forming processes. Once oligodendrocytes and myelin sheaths had been degraded, lipid rich debris must remain. To date, there is no specific data about the distribution and amount of myelin debris during the initiation of MS, although it might be a significant risk factor in launching inflammatory processes. To preserve chemical composition of myelin debris, we used the non-destructive coherent anti-Stokes Raman scattering (CARS) microscopy, a label-free imaging method capable of detecting specific molecules in living tissues by exciting the characteristic intrinsic vibrational frequency of its molecular bond (Cheng et al., 2002; Fu et al., 2008; Haluszka et al., 2015; Hellerer et al., 2007; Saar et al., 2010). We focused femtosecond pulsed laser beams combining 796 nm "pump" and 1028 nm "Stokes" beams to acquire excitation of vibration resonance of CH_2 bonds of lipid molecules. Based on CARS imaging, we quantitatively analysed lipid distribution in different areas of acute brain slices of untreated animals, then we induced myelin degradation in C57BL/6 mice using cuprizone to induce demyelination. Lipid imaging with CARS microscopy on living *in vitro* brain slice preparations show that mild demyelination causes a decrease in the lipid content of white matter leading to the emergence of lipid droplets in the extracellular space. Thus, progression in oligodendrocyte death can cause extensive myelin degradation coupled to the formation of an abundant mass of phagocyted lipid residue.

Methods

Animals, cuprizone treatment and brain slice preparation.

All procedures were performed according to the National Institutes of Health Guide to the Care and Use of Laboratory Animals with the approval of the University of Szeged Ethical Committee and Regional Human Investigation Review Board (ref. 75/2014).
C57BL/6 male mice were used in this study obtained from Charles River (Germany). Animals had *ad libitum* access to standard mouse chow and water. 8 week old mice were treated with cuprizone (Sigma-Aldrich) to induce demyelination (Acs and Kalman, 2012; Blakemore, 1973; Matsushima and Morell, 2001) for up to 5 weeks. 0.2% cuprizone was mixed in the

standard chow of mice. Mice were anaesthetized by inhalation of halothane, and following decapitation 250 µm thick coronal slices were prepared from the somatosensory cortex with a vibrating blade microtome (Microm HM 650 V) immersed in slicing solution containing (in mM): 130 NaCl, 3.5 KCl, 1 NaH_2PO_4, 24 $NaHCO_3$, 1 $CaCl_2$, 3 $MgSO_4$, 10 D(+)-glucose, saturated with 95% O_2 and 5% CO_2. After cutting procedure slices were incubated at room temperature for 1 h in the same solution. The solution used during experiments was identical to the slicing solution, except it contained 3 mM $CaCl_2$ and 1.5 mM $MgSO_4$. During image acquisition slices were kept at ~35˚C.

The human tissue obtained from a 67 years old female patient with written informed consent prior to surgery. Anesthesia was induced with intravenous midazolam and fentanyl (0.03 mg/kg, 1–2 mg/kg, respectively). A bolus dose of propofol (1–2 mg/kg) was administered intravenously. The patients received 0.5 mg/kg rocuronium to facilitate endotracheal intubation. The trachea was intubated and the patient was ventilated with O_2/N_2O mixture at a ratio of 1:2. Anesthesia was maintained with sevoflurane at monitored anesthesia care volume of 1.2–1.5. The biopsy taken from the occipital cortex with a deep brain benign tumour. After surgical removal tissue blocks were immediately immersed in ice-cold slicing solution. Slice preparation was similar as described above, except the thickness of slices were 350 µm.

Coherent anti-Stokes Raman scattering (CARS) Imaging.

A prototype of our experimental setup for CARS imaging was detailed earlier (Haluszka et al., 2015). Our present system included a FemtoCARS Laser Unit and a FemtoFiber Yb-amplifier (both of R&D Ultrafast Lasers Ltd., Hungary), Axio Examiner LSM 7 MP laser scanning 2P microscope (Carl Zeiss, Germany) using 40x water immersion objective (W-Plan, Carl Zeiss, Germany) driven by MaiTai femtosecond pulsing Ti:sapphire laser (Spectra-Physics, Santa Clara, USA). LSM 7 MP microscope was modified for CARS measurements by placing a 650/20 bandpass filter in front of one of the NDDs (non-descanned detector). Anti-Stokes frequency was generated by combining 796 nm pump beam of Ti-sapphire laser and the 1,028 nm Stokes pulses of the Yb-amplifier using dichroic mirror to excite

vibration resonance frequency of CH_2 bond, which is present abundantly in saturated fatty acids offering chemical selectivity to lipids.

Time lapse imaging

Time series Z-stacks CARS images were collected with 60 minutes interval during a 10 hour long image acquisition session from white matter tracks with 0.67 µm z steps with 1024x1024 µm resolution. Stack images were compressed into single image using a maximum projection algorithm.

Fluorescence Labeling

Slices were incubated in a fixating solution which contained 4% paraformaldehyde in 0.1M phosphate buffer (PB; pH=7.4) at 4°C for 3 hours. After several washes in 0.1M PB, slices were cryoprotected with 10% then 20% sucrose solution in 0.1M PB. Slices were frozen three times in liquid nitrogen then embedded in 10% gelatin and further sectioned to 50 µm thick slices. The sections were incubated for one hour in 1 µg/ml BODIPY 493/503 (Thermo Fisher Scientific) in tris-buffered saline (TBS, 0.1M; pH=7.4) at room temperature. The BODIPY 493/503 stock solution (1 mg/ml) was prepared in DMSO. After several washes in 0.1M PB, all sections were mounted in Vectashield (Vector Laboratories) on slides. BODIPY 493/503 fluorescence was visualized using an LSM 880 confocal laser scanning microscope (Carl Zeiss, Germany) with an x40 objective.

Image analysis

Intensity measurements in acquired images were analysed in ZEN (Carl Zeiss, Germany) and ImageJ (NIH, USA) softwares using images of 20 µm depth from the surface of the brain slice. G ratio was calculated as the relation between the inner and outer diameter of the myelinated fiber measured on distinct longitudinal fibers parallel with the image plane without the signs of swelling or degeneration. Z-stack images were acquired with 1 µm steps. Diameters of fibers were acquired from intensity profiles using custom written script in Igor (Wavemetrics, Lake Oswego, USA) by measuring at the level of 70% of the amplitude. Intensity profile of fiber was measured perpendicular of the

middle plane of the fiber. For detecting and measuring number and volume of lipid debris we used a custom written image stack analysis program using C++ language. The program after processing the z-stack images by spatial filtering and thresholding, performed 3D particle separation considering that particles are distinct and globose shaped. Then volume of separated particles were determined based on pixel content.

Statistical analysis

All values are given as mean±standard deviation (s.d.) Statistical significance was tested as defined for each paradigm; Differences with $P<0.05$ were considered significant.

Results

A custom-made coherent anti-Stokes Raman scattering (CARS) microscope (Fu et al., 2011, 2007; Haluszka et al., 2015) equipped with a 40x water immersion objective was used to detect lipid rich structures in acute brain slices of 8 week old C57BL/6 mice. By excitation of the CH_2 bonds in lipids with synchronised laser beams, we aimed to map and characterize lipid distribution in areas of white matter and to reveal the structure and dimensions of myelin sheaths. In order to confirm that the CARS signal was based on lipids, we performed a histochemical staining of neutral lipids with the dye boron-dipyrromethene (BODIPY) on fixed brain slices and detected matching patterns of CARS imaging and BODIPY staining in corpus callosum and layer 6 of somatosensory cortex grey matter (Figure 1A-C).

In order to study applicability of the CARS method in clinical investigations, we performed CARS imaging on acute slices prepared from a human surgical sample. The biopsy taken from the occipital cortex of a 67 years old female patient with a deep brain benign tumour was sliced (350 µm thick) in order to perform *in vitro* imaging. To test long term viability of CARS imaging, time series image Z-stacks were collected during a 10 hour image acquisition session (see methods). We measured G-ratios (ratio of the inner diameter to the outer diameter of the myelin) on healthy fibres and found

no significant differences during the time course of experiments (P=0.57, t-test, 0.45±0.1, n=28 vs. 0.46±0.12, n=32 at the start vs. at 600th minute of recording, respectively) (Figure 1D).

To assess the lipid density of different brain areas, we measured the average pixel intensity of CARS images in equally sized square shaped regions (100 μm^2). We found differences in average CARS signal intensities between different brain areas. Densities of lipids of measured brain areas were significantly different (ANOVA: P<0.001) and decreased in the following order: genu of corpus callosum (CC) > cerebellum (CB) > forceps minor of corpus callosum (FM) > anterior commissure (CA) > subgranular layers of grey matter at primary somatosensory cortex (GM) (Figure 2A, B). When comparing measured areas of white matter tracts, a 3-fold difference was found between the highest (CC) and lowest (CA) lipid content. Relative to the grey matter in the primary somatosensory cortex, areas of white matter showed a 1.2-3.6-fold (CA/GM and CC/GM, respectively) higher in average CARS signals.

Having detected CARS signals in control animals, we proceeded in an experimental model of demyelination. We induced lesions of oligodendrocytes using the toxin cuprizone according to an induced demyelination model of the mouse brain well characterized in the hippocampus, white matter (Acs and Kalman, 2012; Goldberg et al., 2015; Imitola et al., 2011; Komoly, 2005; Koutsoudaki et al., 2009; Silvestroff et al., 2012; Skripuletz et al., 2008). C57BL/6 mice were treated for 4-5 weeks with 0.2% cuprizone mixed in ground chow with free access to food. We performed CARS imaging in cuprizone treated animals and found a significant decrease in averaged pixel intensities of CARS signals of the selected areas (Fig 2B) (Mann-Whitney U test: P<0.001). Normalized to control measurements treatment decreased CARS signals in a brain region dependent manner to 84.2% - 34.2%. Maximal reduction of lipid content was found in the corpus callosum where 34.2% of control signals were detected following the treatment. The ratio of myelin degradation was correlated with control intensities measured in control i.e. areas with higher lipid content in control conditions were the most affected by treatment (Figure 2C).

We monitored demyelination on the single fiber level with CARS imaging of the corpus callosum by measuring the change in G-ratios of longitudinally running axonal fibers without the presence of intramyelinic vacuoles or other morphological signs of degeneration. Corroborating results of earlier studies (Lindner et al., 2008; Silvestroff et al., 2012), we found a significant decrease in G-ratios after cuprizone treatment (0.52 ± 0.11, n=92; t test, $p<0.001$) relative to control (0.43 ± 0.09, n=115; Figure 2D).

An observation based on CARS imaging was the detection of lipid droplets in cuprizone treated animals. A surprisingly rich presence of lipid debris (Figures 2A, 3A) along myelinated fibers in the form of globose particles with a diameter of 0.3-2 µm was detected in each brain areas imaged from all animals. We quantified the amount of lipid particles in two ways: (1) counting the number of distinct droplets and (2) measuring 3D volume of droplets as detailed in the methods section. The number and overall volume of lipid droplets showed similar tendencies and were different between distinct brain areas. In cuprizone treated animals the number (21.38 ± 23.29 particle/$10^4\mu m^3$) and volume (1.1 ± 1.14 μm^3/500 μm^3) of lipid droplets was highest in the richly myelinated corpus callosum ($P<0.001$, one sample Wilcoxon signed-rank test) and lowest in the cerebellum (number, 5.8 ± 8.94 particle/$10^4\mu m^3$; volume, 0.22 ± 0.43 μm^3/500 μm^3; Figure 3). The magnitude of lipid debris accumulation across various brain regions (CC > FM > CA > GM, excluding CB as discussed below) reflected the amounts of intact lipids detected. Moreover, we measured the average pixel intensity of CARS images of different brain areas (excluding debris) and compared with the amount of debris in the same area. We found significant negative correlation between background lipid content of debris free areas and volume of accumulated debris (Figure 3D) (Pearson's r = -0.75) suggesting the transformation of damaged myelin to droplets of lipid debris.

Discussion

Mechanistic understanding of the early stages of MS is incomplete and debated. Appearance of the first clinical symptoms is usually coupled with the escalation of the disease, thus detection of the

initial phase of MS is challenging. We focused on monitoring of myelin sheath breakdown using *in situ*, nondestructive CARS imaging on different brain areas in ex vivo brain slice preparations. We analysed baseline lipid content in different brain areas: subgranular layers of the somatosensory cortex and white matter tracts of the mouse brain: corpus callosum, forceps minor, anterior commisure and cerebellar white matter. As expected, the corpus callosum, being the most heavily myelinated area, produced the most intense CARS signals compared to other brain areas, and the relatively scarcely myelinated grey matter showed the lowest CARS intensity.

Oligodendrocytes have a high lipid content (70-85%) (Hildebrand et al., 1993; Quarles et al., 2006), therefore apoptosis of these cells and breakdown of the myelin sheath leads to the accumulation of lipid debris. Lipid breakdown, however, has not been monitored directly by demyelination studies based on immunohistochemical markers of glial proteins (e.g. proteolipid protein, myelin basic protein etc.) (Clarner et al., 2012; Gudi et al., 2009; Komoly, 2005; Lindner et al., 2008; Safaiyan et al., 2016; Skripuletz et al., 2013; Vogel et al., 2013). The method applied here has several advantages relative to earlier approaches. Signal detection with CARS microscopy allows direct and quantifiable lipid measurements. Moreover, CARS microscopy can be performed in living tissue *in situ* without tissue damage due to the use of multiphoton lasers by tuning our setup for the detection of CH_2 molecular bonds which occur predominantly in lipids. Furthermore, this method is free of potentially lipid damaging chemical postprocessing required for immunocytochemical or histochemical studies (Sommer and Schachner, 1981). Being a confocal imaging method, three dimensional reconstructions and measurements are inherent to CARS imaging.

Cuprizone treatment applied to initiate selective oligodendrogliopathy in mice is an effective, well described and widely used model of MS (Acs and Kalman, 2012; Gudi et al., 2014; Kipp et al., 2009; Matsushima and Morell, 2001) working through the disruption of mitochondrial function followed by the decomposition of the myelin sheath. Demyelination was shown to be specific to brain regions (Goldberg et al., 2015; Gudi et al., 2009; Komoly, 2005; Koutsoudaki et al., 2009; Maña et al., 2009;

Matsushima and Morell, 2001; Silvestroff et al., 2012; Skripuletz et al., 2008) which was recently monitored through microglia and astroglia immunohistochemistry (Goldberg et al., 2015). Cuprizone acts particularly in the heavily myelinated corpus callosum but also affects other brain areas: cerebellar nuclei, optic tracts, hippocampus, putamen, and gray matter areas. The cerebellum appears to respond differently to cuprizone treatment (Groebe et al., 2009; Lampron et al., 2015): extensive demyelination was observed in deep cerebellar nuclei, but white matter tracts remained weakly affected (Groebe et al., 2009). Our experiments show cuprizone induced oligodendropathy and myelin destruction using a noninvasive method of detection *in situ*. We also confirmed demyelination by measuring single fiber thickness and calculating G-ratios. Similar to other studies (Lindner et al., 2008; Silvestroff et al., 2012) cuprizone caused an increase of the G-ratio indicating the reduction of myelin sheath. Elements of the cuprizone model applied here are known to deviate from chronic human MS, for example infiltration of T- and B-cells is inhibited (Emerson et al., 2001; Maña et al., 2009). Nevertheless, cuprizone treatment in mice is considered as a useful model to study early stages of demyelination revealing an increase in the levels of cytokines and neurotrophic factors (Gudi et al., 2009; Matsushima and Morell, 2001; Tanaka et al., 2013) and inducing astrogliosis and microglia recruitment (Clarner et al., 2012; Goldberg et al., 2015; Hiremath et al., 1998; Li et al., 2016; Remington et al., 2007). Activation of microglia is important step in the pathogenesis of myelin disorders through the production of intrinsic mediators of cytotoxicity like nitric oxide, oxygen radicals, glutamate (Neumann et al., 2008; Peferoen et al., 2014). On the other hand, microglias are primarily responsible for scavenging damaged or apoptotic cell parts (Neumann et al., 2008; Nimmerjahn et al., 2005).

Taking advantage of our quantifiable method, spatial distribution of lipid granules were found to be clustered with a few scattered single particles. Clustered lipid droplets observed here are reminiscent of a phagocited lipid debris (Prineas and Graham, 1981) detected by electron microscopy in samples taken at progressed stages of MS (Prineas and Graham, 1981) and similar to findings documented by immunocytochemistry on biopsies from human patients (Huizinga et al., 2012). Moreover, the so

called “foamy” macrophages (Peferoen et al., 2014; Smith, 1999) containing neutral lipid droplets, suggested as residuals of lipid phagocytosis, can be readily detected in autopsies of human MS patients (Boven et al., 2006; Vogel et al., 2013). More recently, Safaiyan and co-workers (Safaiyan et al., 2016) showed that lipid degraded by cuprizone treatment turns up in microglia and accumulates over time. Clearance of myelin debris following the loss of oligodendrocytes is a multifaceted process working at variable timescales (Vargas and Barres, 2007). Proteins are degraded within days e.g. myelin–oligodendrocyte glycoproteins (MOG) and myelin-associated glycoproteins (MAG) are degraded in 3 days, other proteins such as myelin basic protein (MBP) and proteolipid protein (PLP) takes approximately 10 days to eliminate (Brück et al., 1995). Lipid degradation, however, takes much longer and needs presumably more than a year (Adams, 1989), e.g. lipid granules were detected after 9 months after cuprizone induced demyelination (Safaiyan et al., 2016).

Mechanistically, MS is thought to be initiated by autoimmune elements with a major role of $CD4^+$ and $CD8^+$ T cells and additional contribution of other immune cells and pro-inflammatory molecules like cytokines (Noseworthy et al., 2000). It is yet to be decided whether the traditional immune-mediated hypothesis or a more recently suggested alternative, the so called inside-out model explains the onset of MS (Stys et al., 2012). The inside-out model unfolded from studies on autopsies of still myelinated tissue regions of MS patients with apoptotic loss of oligodendrocytes showing microglial activation but without signs of T and B cell infiltration (Barnett and Prineas, 2004; Barnett and Sutton, 2006). The pathogenesis of MS has different variants and complex etiology compromising different stages (Van Der Valk and De Groot, 2000). Cuprizone is an effective tool to study the early stage of MS and, in particular the process of oligodendrocyte lesion and formation and elimination of myelin debris. Trigger event(s) of MS are not clear. According to the inside-out hypothesis, direct oligodendrogliopathy induced by a causative agent is feasible. A recently identified candidate compound in such a process is the toxin of *Clostridium perfrigens* type B known to cause specific oligodendrocyte death (Linden et al., 2015; Rumah et al., 2013). Alternatively, scavenger macrophages entering the brain were hypothesized to be directed against surface components and

cause myelin destruction (Smith, 1999; van der Valk and Amor, 2009). It is speculated that blood derived macrophage or microglia might react against myelin without a known mechanism initiating the process. Our results show the accumulation of lipid droplets which can turn into a subsequent agglomeration at later stages. Recent observations demonstrating the lack of immune response against slowly degrading myelin during the first 40 weeks of oligodendrocyte loss and demyelination (Traka et al., 2015) suggest that the onset of oligodendrocyte death is likely to be independent of the complement system. Clustering of lipid droplets is consistent with the involvement of macrophages and generation of inflammation (Wang et al., 2015). Inflammation in the CNS can be induced by sulfatide, a major component of myelin sheath (Jeon et al., 2008) and lipid laden macrophages can generate a chronic inflammatory state in the spinal cord (Wang et al., 2015). Moreover, recent studies showed that injection of homogenized lipid debris into the brain generates enormous microglia recruitment and triggers inflammatory responses (Clarner et al., 2012; Sun et al., 2010). When lipids are released from dying myelin sheaths, they might exacerbate the condition by inhibiting CNS remyelination (Kotter, 2006; Lampron et al., 2015). Thus, our measurements suggest that oligodendrocyte death in the cuprizone model of MS may followed by the gradual accumulation of sporadic lipid droplets without rapid degradation of their lipid content which eventually can lead to lipid droplet agglomeration in macrophages and onset of inflammation.

Legends to Figures

Figure 1. CARS intensity reflects lipid rich structures in cortical slice of mouse and human. (A) Diagram shows control coronal brain section. Red and blue outlines indicate imaged areas shown in A and B, respectively. (B) Top: Representative CARS image of corpus callosum from mouse brain slice. Bottom: Same sample histochemical staining with BODIPY. (C) Left: Representative CARS image of corpus callosum from mouse brain slice. Right: Same sample stained with BODIPY. Note the similar fiber patterns on the left side of images. (D) Representative CARS images of white matter of cortical

slice from biopsy of human patient before (left) and after (right) long term in vitro recording session. Scalebars, 20 µm.

Figure 2. Detection of demyelination with CARS in cuprizone treated animals. (A) Representative CARS images of control (left) and 0.2% cuprizone (right) treated sample from corpus callosum. (B) Quantification of myelin density by measuring averaged total CARS intensity of selected areas of brain slices from control (left) and 0.2% cuprizone (right) treated mice. (C) Scatter plots showing the average pixel intensity values comparing with loss of lipid during different concentrations of treatments. Cerebellar data point (hollow symbol) was excluded from line fit (see discussion). (D) Cuprizone treatment induce change of G-ratio of myelin sheath. Images are representative examples of images of myelin sheaths in control (left) and 0.2% (right) cuprizone treatment. CARS pixel intensity were measured along profiles indicated with white lines perpendicular to fibers. Scalebars, (A) 20 µm; (D) 5 µm. Mann-Whitney U test: ***$p<0.001$

Figure 3. Quantification of accumulated myelin debris in white matter structures. (A) Representative photos showing CARS signal images brain slices acquired from control (left) and 0.2% cuprizone treated (right) animals from brain areas indicated on the top drawings. Red arrows indicate solitary and conglomerates of myelin debris. (B) Representative sample of 3D volume reconstruction of image stack (71x71x10 µm) originate from a cuprizone treated animal. (C) Quantification of number and volume of myelin debris in different brain regions after 0.2% cuprizone treatment. (D) Scattergram shows negative correlation of measured lipid debris number and measured CARS intensity in corpus callosum cuprizone treated tissue. Scalebars, 10 µm.CA anterior commissure

CARS coherent anti-Stokes Raman scattering

CB cerebellum

CC corpus callosum

CNS central nervous sytem

FM forceps minor of corpus callosum

GM grey matter

MAG myelin-associated glycoproteins

MOG myelin–oligodendrocyte glycoproteins

EAE experimental autoimmune encephalomyelitis

GWAS genome-wide association studies

Ethics approval and consent to participate

All procedures were performed according to the National Institutes of Health Guide to the Care and Use of Laboratory Animals with the approval of the University of Szeged Ethical Committee and Regional Human Investigation Review Board (ref. 75/2014).

Competing interests

RS has a share in R&D Ultrafast Lasers Ltd.

Acknowledgement

We would like to thank to Mariann Gyengéné Ruszka and Katalin Mikite for their excellent technical assistance and Dr Bernadette Kálmán for her comments on the MS.

Funding

This research was supported by the Hungarian Academy of Sciences, the Hungarian Brain Research Program (KTIA_13_NAP-A-I/16), the European Research Council Advanced Grant (INTERIMPACT) project and R&D Ultrafast Lasers Ltd.

Author contributions statement

AO, JB and GM performed the experiment. RS and GT and GM optimized the microscope and laser setup for CARS. AO, ZO and GM evaluated the data. GT and GM wrote the manuscript. All authors read and approved the final manuscript.

References

Acs, P., Kalman, B., 2012. Autoimmunity, Methods in Molecular Biology. Humana Press, Totowa, NJ. doi:10.1007/978-1-60761-720-4

Adams, C.W.M., 1989. A Colour Atlas of Multiple Sclerosis and Disorders of Myelin [Mosby].

Bando, Y., Takakusaki, K., Ito, S., Terayama, R., Kashiwayanagi, M., Yoshida, S., 2008. Differential changes in axonal conduction following CNS demyelination in two mouse models. Eur. J. Neurosci. 28, 1731–42. doi:10.1111/j.1460-9568.2008.06474.x

Barnett, M.H., Prineas, J.W., 2004. Relapsing and remitting multiple sclerosis: Pathology of the newly forming lesion. Ann. Neurol. 55, 458–468. doi:10.1002/ana.20016

Barnett, M.H., Sutton, I., 2006. The pathology of multiple sclerosis: a paradigm shift. Curr. Opin. Neurol. 19, 242–247. doi:10.1097/01.wco.0000227032.47458.cb

Blakemore, W.F., 1973. Demyelination of the superior cerebellar peduncle in the mouse induced by cuprizone. J. Neurol. Sci. 20, 63–72. doi:10.1016/0022-510X(73)90118-4

Boven, L.A., Van Meurs, M., Van Zwam, M., Wierenga-Wolf, A., Hintzen, R.Q., Boot, R.G., Aerts, J.M., Amor, S., Nieuwenhuis, E.E., Laman, J.D., 2006. Myelin-laden macrophages are anti-inflammatory, consistent with foam cells in multiple sclerosis. Brain 129, 517–526. doi:10.1093/brain/awh707

Brück, W., Porada, P., Poser, S., Rieckmann, P., Hanefeld, F., Kretzschmar, H.A., Lassmann, H., 1995. Monocyte/macrophage differentiation in early multiple sclerosis lesions. Ann. Neurol. 38, 788–796. doi:10.1002/ana.410380514

Centonze, D., Muzio, L., Rossi, S., Furlan, R., Bernardi, G., Martino, G., 2010. The link between inflammation, synaptic transmission and neurodegeneration in multiple sclerosis. Cell Death Differ. 17, 1083–1091. doi:10.1038/cdd.2009.179

Cheng, J., Jia, Y., Zheng, G., Xie, X., 2002. Laser-scanning coherent anti-Stokes Raman scattering microscopy and applications to cell biology. Biophys. J. doi:10.1016/S0006-3495(02)75186-2

Clarner, T., Diederichs, F., Berger, K., Denecke, B., Gan, L., van der Valk, P., Beyer, C., Amor, S., Kipp, M., 2012. Myelin debris regulates inflammatory responses in an experimental demyelination animal model and multiple sclerosis lesions. Glia 60, 1468–1480. doi:10.1002/glia.22367

Emerson, M.R., Biswas, S., LeVine, S.M., 2001. Cuprizone and piperonyl butoxide, proposed inhibitors of T-cell function, attenuate experimental allergic encephalomyelitis in SJL mice. J. Neuroimmunol. 119, 205–213. doi:10.1016/S0165-5728(01)00394-0

Frohman, E.M., Racke, M.K., Raine, C.S., 2006. Multiple sclerosis--the plaque and its pathogenesis. N. Engl. J. Med. 354, 942–955. doi:10.1056/NEJMra052130

Fu, Y., Frederick, T.J., Huff, T.B., Goings, G.E., Miller, S.D., Cheng, J.-X., 2011. Paranodal myelin retraction in relapsing experimental autoimmune encephalomyelitis visualized by coherent anti-Stokes Raman scattering microscopy. J. Biomed. Opt. 16, 106006. doi:10.1117/1.3638180

Fu, Y., Huff, T.B., Wang, H.-W., Wang, H., Cheng, J.-X., 2008. Ex vivo and in vivo imaging of myelin fibers in mouse brain by coherent anti-Stokes Raman scattering microscopy. Opt. Express 16, 19396–409.

Fu, Y., Wang, H., Huff, T.B., Shi, R., Cheng, J., 2007. Coherent anti-Stokes Raman scattering imaging of myelin degradation reveals a calcium-dependent pathway in lyso-PtdCho-induced demyelination. J. Neurosci. Res. 85, 2870–81. doi:10.1002/jnr.21403

Goldberg, J., Clarner, T., Beyer, C., Kipp, M., 2015. Anatomical Distribution of Cuprizone-Induced Lesions in C57BL6 Mice. J. Mol. Neurosci. 166–175. doi:10.1007/s12031-015-0595-5

Groebe, A., Clarner, T., Baumgartner, W., Dang, J., Beyer, C., Kipp, M., 2009. Cuprizone treatment induces distinct demyelination, astrocytosis, and microglia cell invasion or proliferation in the mouse cerebellum. Cerebellum 8, 163–174. doi:10.1007/s12311-009-0099-3

Gudi, V., Gingele, S., Skripuletz, T., Stangel, M., 2014. Glial response during cuprizone-induced de- and remyelination in the CNS: lessons learned. Front. Cell. Neurosci. 8, 73. doi:10.3389/fncel.2014.00073

Gudi, V., Moharregh-Khiabani, D., Skripuletz, T., Koutsoudaki, P.N., Kotsiari, A., Skuljec, J., Trebst, C., Stangel, M., 2009. Regional differences between grey and white matter in cuprizone induced demyelination. Brain Res. 1283, 127–138. doi:10.1016/j.brainres.2009.06.005

Haluszka, D., Lőrincz, K., Molnár, G., Tamás, G., Kolonics, A., Szipőcs, R., Kárpáti, S., Wikonkál, N.M., 2015. *In vivo* second-harmonic generation and *ex vivo* coherent anti-stokes raman scattering microscopy to study the effect of obesity to fibroblast cell function using an Yb-fiber laser-based CARS extension unit. Microsc. Res. Tech. 78, 823–830. doi:10.1002/jemt.22545

Hamada, M.S., Kole, M.H.P., 2015. Myelin Loss and Axonal Ion Channel Adaptations Associated with Gray Matter Neuronal Hyperexcitability. J. Neurosci. 35, 7272–7286. doi:10.1523/JNEUROSCI.4747-14.2015

Hellerer, T., Axäng, C., Brackmann, C., Hillertz, P., Pilon, M., Enejder, A., 2007. Monitoring of lipid storage in Caenorhabditis elegans using coherent anti-Stokes Raman scattering (CARS) microscopy. Proc. Natl. Acad. Sci. U. S. A. 104, 14658–14663. doi:10.1073/pnas.0703594104

Hemmer, B., Archelos, J.J., Hartung, H.-P., 2002. New Concepts in the Immunopathogenesis of Multiple Sclerosis. Nat. Rev. Neurosci. 3, 291–301. doi:10.1038/nrn784

Hildebrand, C., Remahl, S., Persson, H., Bjartmar, C., 1993. Myelinated nerve fibres in the CNS. Prog. Neurobiol. 40, 319–384. doi:10.1016/0301-0082(93)90015-K

Hiremath, M.M., Saito, Y., Knapp, G.W., Ting, J.P.Y., Suzuki, K., Matsushima, G.K., 1998.

Microglial/macrophage accumulation during cuprizone-induced demyelination in C57BL/6 mice. J. Neuroimmunol. 92, 38–49. doi:10.1016/S0165-5728(98)00168-4

Huizinga, R., van der Star, B.J., Kipp, M., Jong, R., Gerritsen, W., Clarner, T., Puentes, F., Dijkstra, C.D., van der Valk, P., Amor, S., 2012. Phagocytosis of neuronal debris by microglia is associated with neuronal damage in multiple sclerosis. Glia 60, 422–31. doi:10.1002/glia.22276

Imitola, J., Côté, D., Rasmussen, S., Xie, X.S., Liu, Y., Chitnis, T., Sidman, R.L., Lin, C.P., Khoury, S.J., 2011. Multimodal coherent anti-Stokes Raman scattering microscopy reveals microglia-associated myelin and axonal dysfunction in multiple sclerosis-like lesions in mice. J. Biomed. Opt. 16, 21109. doi:10.1117/1.3533312

Jeon, S.-B., Yoon, H.J., Park, S.-H., Kim, I.-H., Park, E.J., 2008. Sulfatide, a major lipid component of myelin sheath, activates inflammatory responses as an endogenous stimulator in brain-resident immune cells. J. Immunol. 181, 8077–8087. doi:181/11/8077 [pii]

Kipp, M., Clarner, T., Dang, J., Copray, S., Beyer, C., 2009. The cuprizone animal model: New insights into an old story. Acta Neuropathol. 118, 723–736. doi:10.1007/s00401-009-0591-3

Komoly, S., 2005. Experimental demyelination caused by primary oligodendrocyte dystrophy. Regional distribution of the lesions in the nervous system of mice [corrected]. Ideggyogy. Sz. 58, 40–3.

Kornek, B., Lassmann, H., 2003. Neuropathology of multiple sclerosis - New concepts. Brain Res. Bull. 61, 321–326. doi:10.1016/S0361-9230(03)00095-9

Kotter, M.R., 2006. Myelin Impairs CNS Remyelination by Inhibiting Oligodendrocyte Precursor Cell Differentiation. J. Neurosci. 26, 328–332. doi:10.1523/JNEUROSCI.2615-05.2006

Koutsoudaki, P.N., Skripuletz, T., Gudi, V., Moharregh-Khiabani, D., Hildebrandt, H., Trebst, C., Stangel, M., 2009. Demyelination of the hippocampus is prominent in the cuprizone model. Neurosci. Lett. 451, 83–8. doi:10.1016/j.neulet.2008.11.058

Kuhlmann, T., Lingfeld, G., Bitsch, A., Schuchardt, J., Brück, W., 2002. Acute axonal damage in multiple sclerosis is most extensive in early disease stages and decreases over time. Brain 125, 2202–2212. doi:10.1093/brain/awf235

Lampron, A., Larochelle, A., Laflamme, N., Prefontaine, P., Plante, M.-M., Sanchez, M.G., Yong, V.W., Stys, P.K., Tremblay, M.-E., Rivest, S., 2015. Inefficient clearance of myelin debris by microglia impairs remyelinating processes. J. Exp. Med. 212, 481–495. doi:10.1084/jem.20141656

Li, J., Zhang, L., Chu, Y., Namaka, M., Deng, B., Kong, J., Bi, X., 2016. Astrocytes in Oligodendrocyte Lineage Development and White Matter Pathology. Front. Cell. Neurosci. 10, 1–13. doi:10.3389/fncel.2016.00119

Linden, J.R., Ma, Y., Zhao, B., Harris, J.M., Rumah, K.R., Schaeren-Wiemers, N., Vartanian, T., 2015. Clostridium perfringens Epsilon Toxin Causes Selective Death of Mature Oligodendrocytes and Central Nervous System Demyelination. MBio 6, e02513-14-. doi:10.1128/mBio.02513-14

Lindner, M., Fokuhl, J., Linsmeier, F., Trebst, C., Stangel, M., 2009. Chronic toxic demyelination in the central nervous system leads to axonal damage despite remyelination. Neurosci. Lett. 453, 120–5. doi:10.1016/j.neulet.2009.02.004

Lindner, M., Heine, S., Haastert, K., Garde, N., Fokuhl, J., Linsmeier, F., Grothe, C., Baumgärtner, W., Stangel, M., 2008. Sequential myelin protein expression during remyelination reveals fast and efficient repair after central nervous system demyelination. Neuropathol. Appl. Neurobiol. 34, 105–114. doi:10.1111/j.1365-2990.2007.00879.x

Maña, P., Fordham, S. a, Staykova, M. a, Correcha, M., Silva, D., Willenborg, D.O., Liñares, D., 2009. Demyelination caused by the copper chelator cuprizone halts T cell mediated autoimmune neuroinflammation. J. Neuroimmunol. 210, 13–21. doi:10.1016/j.jneuroim.2009.02.013

Matsushima, G.K., Morell, P., 2001. The neurotoxicant, cuprizone, as a model to study demyelination and remyelination in the central nervous system. Brain Pathol. 11, 107–116.

doi:10.1111/j.1750-3639.2001.tb00385.x

Merrill, J.E., 2009. In vitro and in vivo pharmacological models to assess demyelination and remyelination. Neuropsychopharmacology 34, 55–73. doi:10.1038/npp.2008.145

Neumann, H., Kotter, M.R., Franklin, R.J.M., 2008. Debris clearance by microglia: an essential link between degeneration and regeneration. Brain 132, 288–295. doi:10.1093/brain/awn109

Nimmerjahn, A., Kirchhoff, F., Helmchen, F., 2005. Resting microglial cells are highly dynamic surveillants of brain parenchyma in vivo. Science 308, 1314–8. doi:10.1126/science.1110647

Noseworthy, J.H., Lucchinetti, C., Rodriguez, M., Weinshenker, B.G., 2000. Multiple Sclerosis. N. Engl. J. Med. 343, 938–952. doi:10.1056/NEJM200009283431307

Peferoen, L., Kipp, M., van der Valk, P., van Noort, J.M., Amor, S., 2014. Oligodendrocyte-microglia cross-talk in the central nervous system. Immunology 141, 302–313. doi:10.1111/imm.12163

Prineas, J.W., Graham, J.S., 1981. Multiple sclerosis: capping of surface immunoglobulin G on macrophages engaged in myelin breakdown. Ann. Neurol. 10, 149–58. doi:10.1002/ana.410100205

Quarles, R.H., Macklin, W.B., Morell, P., 2006. Myelin Formation, Structure and Biochemistry. Basic Neurochem. Mol. Cell. Med. Asp. 51–71. doi:10.1042/BJ20110539

Ransohoff, R.M., 2012. Animal models of multiple sclerosis: the good, the bad and the bottom line. Nat. Neurosci. 15, 1074–7. doi:10.1038/nn.3168

Remington, L.T., Babcock, A. a, Zehntner, S.P., Owens, T., 2007. Microglial recruitment, activation, and proliferation in response to primary demyelination. Am. J. Pathol. 170, 1713–1724. doi:10.2353/ajpath.2007.060783

Rumah, K.R., Linden, J., Fischetti, V.A., Vartanian, T., 2013. Isolation of Clostridium perfringens Type B in an Individual at First Clinical Presentation of Multiple Sclerosis Provides Clues for

Environmental Triggers of the Disease. PLoS One 8. doi:10.1371/journal.pone.0076359

Saar, B.G., Freudiger, C.W., Reichman, J., Stanley, C.M., Holtom, G.R., Xie, X.S., 2010. Video-rate molecular imaging in vivo with stimulated Raman scattering. Science 330, 1368–1370. doi:10.1126/science.1197236

Safaiyan, S., Kannaiyan, N., Snaidero, N., Brioschi, S., Biber, K., Yona, S., Edinger, A.L., Jung, S., Rossner, M.J., Simons, M., 2016. Age-related myelin degradation burdens the clearance function of microglia during aging. Nat. Neurosci. 1–7. doi:10.1038/nn.4325

Sawcer, S., Hellenthal, G., Pirinen, M., Spencer, C.C.A., Patsopoulos, N. a, Moutsianas, L., Dilthey, A., Su, Z., Freeman, C., Hunt, S.E., Edkins, S., Gray, E., Booth, D.R., Potter, S.C., Goris, A., Band, G., Oturai, A.B., Strange, A., Saarela, J., Bellenguez, C., Fontaine, B., Gillman, M., Hemmer, B., Gwilliam, R., Zipp, F., Jayakumar, A., Martin, R., Leslie, S., Hawkins, S., Giannoulatou, E., D'alfonso, S., Blackburn, H., Martinelli Boneschi, F., Liddle, J., Harbo, H.F., Perez, M.L., Spurkland, A., Waller, M.J., Mycko, M.P., Ricketts, M., Comabella, M., Hammond, N., Kockum, I., McCann, O.T., Ban, M., Whittaker, P., Kemppinen, A., Weston, P., Hawkins, C., Widaa, S., Zajicek, J., Dronov, S., Robertson, N., Bumpstead, S.J., Barcellos, L.F., Ravindrarajah, R., Abraham, R., Alfredsson, L., Ardlie, K., Aubin, C., Baker, A., Baker, K., Baranzini, S.E., Bergamaschi, L., Bergamaschi, R., Bernstein, A., Berthele, A., Boggild, M., Bradfield, J.P., Brassat, D., Broadley, S. a, Buck, D., Butzkueven, H., Capra, R., Carroll, W.M., Cavalla, P., Celius, E.G., Cepok, S., Chiavacci, R., Clerget-Darpoux, F., Clysters, K., Comi, G., Cossburn, M., Cournu-Rebeix, I., Cox, M.B., Cozen, W., Cree, B. a C., Cross, A.H., Cusi, D., Daly, M.J., Davis, E., de Bakker, P.I.W., Debouverie, M., D'hooghe, M.B., Dixon, K., Dobosi, R., Dubois, B., Ellinghaus, D., Elovaara, I., Esposito, F., Fontenille, C., Foote, S., Franke, A., Galimberti, D., Ghezzi, A., Glessner, J., Gomez, R., Gout, O., Graham, C., Grant, S.F. a, Guerini, F.R., Hakonarson, H., Hall, P., Hamsten, A., Hartung, H.-P., Heard, R.N., Heath, S., Hobart, J., Hoshi, M., Infante-Duarte, C., Ingram, G., Ingram, W., Islam, T., Jagodic, M., Kabesch, M., Kermode, A.G., Kilpatrick, T.J., Kim, C., Klopp, N.,

Koivisto, K., Larsson, M., Lathrop, M., Lechner-Scott, J.S., Leone, M.A., Leppä, V., Liljedahl, U., Bomfim, I.L., Lincoln, R.R., Link, J., Liu, J., Lorentzen, A.R., Lupoli, S., Macciardi, F., Mack, T., Marriott, M., Martinelli, V., Mason, D., McCauley, J.L., Mentch, F., Mero, I.-L., Mihalova, T., Montalban, X., Mottershead, J., Myhr, K.-M., Naldi, P., Ollier, W., Page, A., Palotie, A., Pelletier, J., Piccio, L., Pickersgill, T., Piehl, F., Pobywajlo, S., Quach, H.L., Ramsay, P.P., Reunanen, M., Reynolds, R., Rioux, J.D., Rodegher, M., Roesner, S., Rubio, J.P., Rückert, I.-M., Salvetti, M., Salvi, E., Santaniello, A., Schaefer, C. a, Schreiber, S., Schulze, C., Scott, R.J., Sellebjerg, F., Selmaj, K.W., Sexton, D., Shen, L., Simms-Acuna, B., Skidmore, S., Sleiman, P.M. a, Smestad, C., Sørensen, P.S., Søndergaard, H.B., Stankovich, J., Strange, R.C., Sulonen, A.-M., Sundqvist, E., Syvänen, A.-C., Taddeo, F., Taylor, B., Blackwell, J.M., Tienari, P., Bramon, E., Tourbah, A., Brown, M. a, Tronczynska, E., Casas, J.P., Tubridy, N., Corvin, A., Vickery, J., Jankowski, J., Villoslada, P., Markus, H.S., Wang, K., Mathew, C.G., Wason, J., Palmer, C.N. a, Wichmann, H.-E., Plomin, R., Willoughby, E., Rautanen, A., Winkelmann, J., Wittig, M., Trembath, R.C., Yaouanq, J., Viswanathan, A.C., Zhang, H., Wood, N.W., Zuvich, R., Deloukas, P., Langford, C., Duncanson, A., Oksenberg, J.R., Pericak-Vance, M.A., Haines, J.L., Olsson, T., Hillert, J., Ivinson, A.J., De Jager, P.L., Peltonen, L., Stewart, G.J., Hafler, D.A., Hauser, S.L., McVean, G., Donnelly, P., Compston, A., 2011. Genetic risk and a primary role for cell-mediated immune mechanisms in multiple sclerosis. Nature 476, 214–9. doi:10.1038/nature10251

Silvestroff, L., Bartucci, S., Pasquini, J., Franco, P., 2012. Cuprizone-induced demyelination in the rat cerebral cortex and thyroid hormone effects on cortical remyelination. Exp. Neurol. 235, 357–67. doi:10.1016/j.expneurol.2012.02.018

Simpson, S., Taylor, B. V., van der Mei, I., 2015. The role of epidemiology in MS research: Past successes, current challenges and future potential. Mult. Scler. J. 969–977. doi:10.1177/1352458515574896

Skripuletz, T., Gudi, V., Hackstette, D., Stangel, M., 2011. De- and remyelination in the CNS white and

grey matter induced by cuprizone: the old, the new, and the unexpected. Histol. Histopathol. 26, 1585–97.

Skripuletz, T., Hackstette, D., Bauer, K., Gudi, V., Pul, R., Voss, E., Berger, K., Kipp, M., Baumg??rtner, W., Stangel, M., 2013. Astrocytes regulate myelin clearance through recruitment of microglia during cuprizone-induced demyelination. Brain 136, 147–167. doi:10.1093/brain/aws262

Skripuletz, T., Lindner, M., Kotsiari, A., Garde, N., Fokuhl, J., Linsmeier, F., Trebst, C., Stangel, M., 2008. Cortical demyelination is prominent in the murine cuprizone model and is strain-dependent. Am. J. Pathol. 172, 1053–61. doi:10.2353/ajpath.2008.070850

Smith, M.E., 1999. Phagocytosis of myelin in demyelinative disease: A review. Neurochem. Res. 24, 261–268. doi:10.1023/A:1022566121967

Sommer, I., Schachner, M., 1981. Monoclonal antibodies (O1 to O4) to oligodendrocyte cell surfaces: An immunocytological study in the central nervous system. Dev. Biol. 83, 311–327. doi:10.1016/0012-1606(81)90477-2

Stadelmann, C., Wegner, C., Brück, W., 2011. Inflammation, demyelination, and degeneration - Recent insights from MS pathology. Biochim. Biophys. Acta - Mol. Basis Dis. 1812, 275–282. doi:10.1016/j.bbadis.2010.07.007

Stys, P.K., Zamponi, G.W., van Minnen, J., Geurts, J.J.G., 2012. Will the real multiple sclerosis please stand up? Nat. Rev. Neurosci. 13, 507–514. doi:10.1038/nrn3275

Sun, X., Wang, X., Chen, T., Li, T., Cao, K., Lu, A., Chen, Y., Sun, D., Luo, J., Fan, J., Young, W., Ren, Y., 2010. Myelin activates FAK/Akt/NF-κB pathways and provokes CR3-dependent inflammatory response in murine system. PLoS One 5. doi:10.1371/journal.pone.0009380

Tanaka, T., Murakami, K., Bando, Y., Yoshida, S., 2013. Minocycline reduces remyelination by suppressing ciliary neurotrophic factor expression after cuprizone-induced demyelination. J. Neurochem. 127, 259–70. doi:10.1111/jnc.12289

Traka, M., Podojil, J.R., McCarthy, D.P., Miller, S.D., Popko, B., 2015. Oligodendrocyte death results in immune-mediated CNS demyelination. Nat. Neurosci. 19, 65–74. doi:10.1038/nn.4193

Trapp, B.D., Nave, K.-A., 2008. Multiple sclerosis: an immune or neurodegenerative disorder? Annu. Rev. Neurosci. 31, 247–69. doi:10.1146/annurev.neuro.30.051606.094313

van der Valk, P., Amor, S., 2009. Preactive lesions in multiple sclerosis. Curr. Opin. Neurol. 22, 207–213. doi:10.1097/WCO.0b013e32832b4c76

Van Der Valk, P., De Groot, C.J. a, 2000. Staging of multiple sclerosis (MS) lesions: Pathology of the time frame of MS. Neuropathol. Appl. Neurobiol. 26, 2–10. doi:10.1046/j.1365-2990.2000.00217.x

Vargas, M.E., Barres, B.A., 2007. Why Is Wallerian Degeneration in the CNS So Slow? Annu. Rev. Neurosci. 30, 153–179. doi:10.1146/annurev.neuro.30.051606.094354

Vogel, D.Y., Vereyken, E.J., Glim, J.E., Heijnen, P.D., Moeton, M., van der Valk, P., Amor, S., Teunissen, C.E., van Horssen, J., Dijkstra, C.D., 2013. Macrophages in inflammatory multiple sclerosis lesions have an intermediate activation status. J. Neuroinflammation 10, 35. doi:10.1186/1742-2094-10-35

Wang, X., Cao, K., Sun, X., Chen, Y., Duan, Z., Sun, L., Guo, L., Bai, P., Sun, D., Fan, J., He, X., Young, W., Ren, Y., 2015. Macrophages in spinal cord injury: Phenotypic and functional change from exposure to myelin debris. Glia 63, 635–651. doi:10.1002/glia.22774

Figure Caption

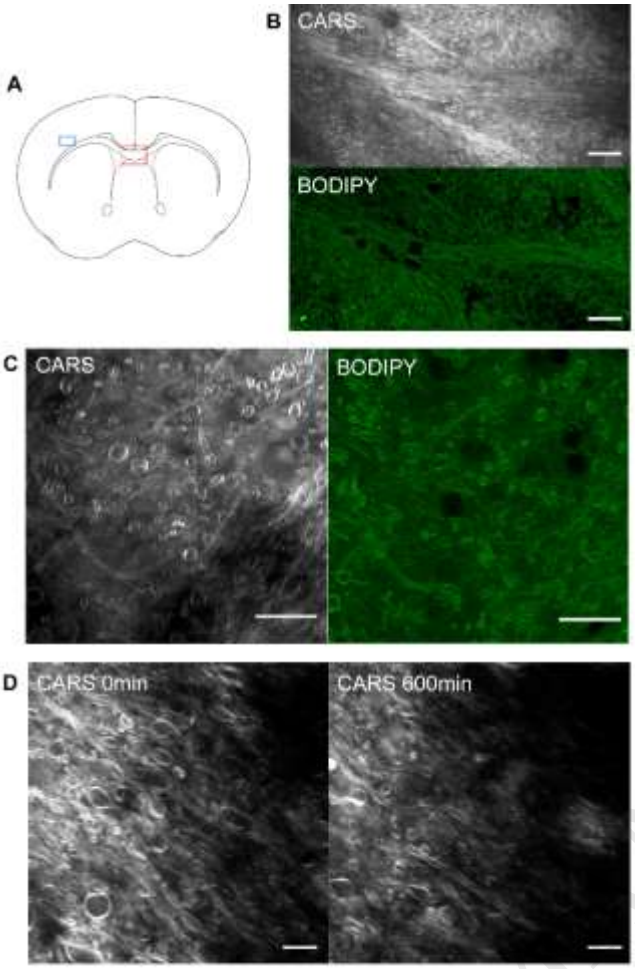

Figr-1

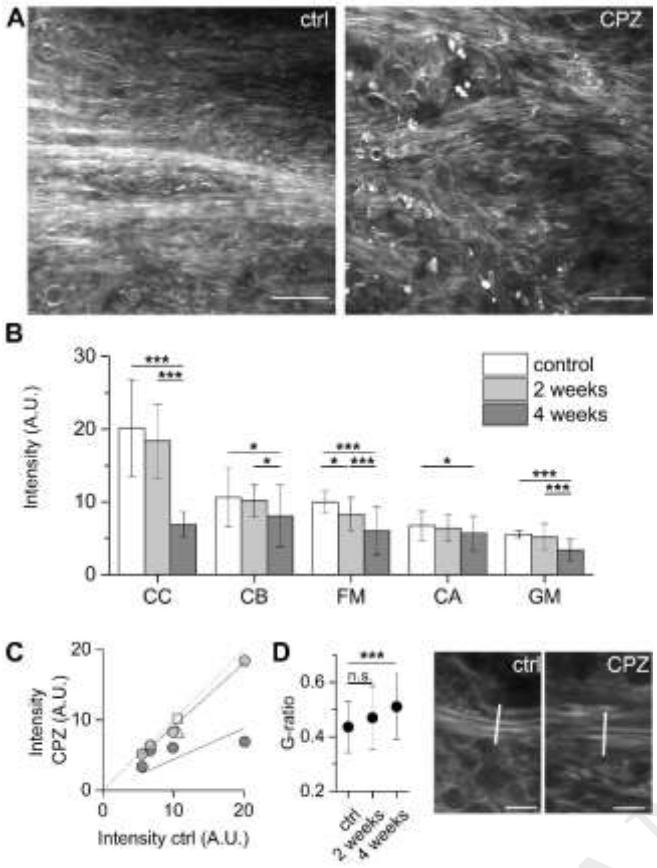

Figr-2

Figr-3